Springer

KSME

Journal of Mechanical Science and Technology 29 (12) (2015) 5167~5181
www.springerlink.com/content/1738-494x(Print)/1976-3824(Online)
DOI 10.1007/s12206-015-1117-7

Analysis of vibro-impacts in a torsional system under both wide open throttle and coast conditions with focus on the multi-staged clutch damper †

Jong-Yun Yoon[1] and Byeongil Kim[2,*]

[1]*Division of Mechanical and Automotive Engineering, Kongju National University, Chungnam, 331-717, Korea*
[2]*School of Mechanical Engineering, Yeungnam University, Gyeongsangbuk-do, 712-749, Korea*

(Manuscript Received March 3, 2015; Revised August 4, 2015; Accepted August 20, 2015)

Abstract

Vibro-impacts of gear pairs in a torsion system inherently occur under the steady state torque input condition since clearance type nonlinearities are related to the torsional vibration induced by the firing stroke of an engine. In order to investigate the dynamic characteristics of gear rattle, front engine and front wheel drive configuration of the manual transmission is investigated under both wide open throttle and coast conditions. This configuration is examined using 6 degree-of-freedom system model, embedded by the relevant nonlinearities such as multi-staged clutch dampers, gear backlash and drag torques. This article focuses on the relationship of vibro-impacts with key parameters of clutch dampers, where the gear rattle phenomena are defined by "sing-sided", "double-sided" and "no-impact" along with different clutch dampers. Thus, the mathematical model of the multi-staged clutch dampers is developed by including the asymmetric transition angles and pre-load effect. Based upon this nonlinear model, three real-life clutch dampers are employed and simulated results are compared with limited experimental measurements conducted on a vehicle. Also, the dynamic characteristics of gear motions under the coast condition are investigated. This coast condition is explained corresponding to different input torque conditions and its simulations show the main reasons of vibro-impacts induced by the clutch stopper well. Finally, modified clutch damper concepts for rattle-free transmission are proposed along with dynamic clutch design guidelines.

Keywords: Vibro-impact; Gear rattle; Multi-staged clutch damper; Asymmetric transition angles; Gear backlash; Drag torque; Coast condition

1. Introduction

Vibro-impacts such as gear rattle in a vehicle driveline system are inherently induced by the engine stroke under various driving conditions. For example, the Wide open throttle (WOT) and idling are defined by the engine firing status. Acceleration or coast conditions are pertaining to the vehicle driving status. The vibratory motions are mostly involved with clearance type nonlinearities in a torsional system and degrade the vehicle sound qualities as well as the durability concerned with the heavy duty engines [1-5]. To find out the dynamic characteristics of gear rattle, three representative vibro-impact types are defined as "single-sided", "double-sided" and "no-impact" [6]. On the basis of the simulated results along with system parameters, the clutch design guide lines for the rattle-free torsional system have been suggested [7].

In addition, the simulation and experimental models for the rattle phenomena have been developed for more than a decade [8-14]. For example, Barthod et al. [8] have conducted rattling test by using the simplified gearbox with a parametric study given different gear inertia, backlash and excitation conditions. Wang et al. [9] have used decoupling procedure by focusing on rattling gear pairs to develop the system model. Shim et al. [10] have investigated an anti-backlash to reduce the rattle noise in an agricultural tractor's driveline. Rocca and Russo [11] have constructed the lab-experiment to examine the rattle phenomena in a gear box. Karagiannis and Pfeiffer [12] have employed classical impact theory and topological dynamic concepts to present the gear rattling phenomena. Bozca and Fietkau [13] have analyzed the relationship between rattle noise and design factors empirically. Tangasawi et al. [14] have considered the contact film reaction and gear flank friction in a front wheel manual transmission with diesel engine. Analytical models with the reduced lump parameter models have been suggested by using harmonic balance method [15-18] and employing impact damping model [19, 20] as well. Also, more researches concerned with vibro-impacts have been reported by pursuing experimental and simulation methods [21-28].

On the basis of the literature review, most of works have been conducted on component levels or simple models. Also, the nonlinear clutch models have been limited on symmetrical

*Corresponding author. Tel.: +82 53 810 2447, Fax.: +82 53 810 4627
E-mail address: bikim@yu.ac.kr
† Recommended by Associate Editor Eung-Soo Shin

types [1-6]. Thus, in this article, two different engine operating conditions will be examined on the levels of vehicle driveline system including asymmetrical types of multi-staged clutch dampers by focusing on the development of simulation method. And gear rattle under WOT and coast conditions will be investigated with three real-life multi-staged clutch dampers. Chief objectives of this article are summarized as follows: 1) develop the mathematical model for the multi-staged clutch dampers with asymmetric transition angles by focusing on the manual transmission; 2) investigate the characteristics of vibro-impacts along with three real-life clutch dampers; 3) suggest the nonlinear simulation models under different vehicle driving conditions such as WOT and coast.

2. Problem formulations

Fig. 1 illustrates a 6 Degree-of-freedom (DOF) Linear time-invariant (LTI) system model which is based upon the vehicle driveline. The procedure of the system reduction can be referred to the prior studies [6, 29]. The employed values and designation of parameters are listed as follows: inertia of flywheel, $I_f = 1.38\times10^{-1}$ kg·m^2; inertia of 1st mass flywheel, $I_{fa} = 0.7\times I_f$ kg·m^2; inertia of 2nd mass flywheel, $I_{fb} = 0.3\times I_f$ kg·m^2; inertia of clutch hub, $I_h = 5.76\times10^{-3}$ kg·m^2; inertia of input shaft, $I_{ie} = 4.53\times10^{-3}$ kg·m^2; inertia of output shaft, $I_{OG} = 5.23\times10^{-4}$ kg·m^2; inertia of unloaded gear, $I_{ou} = 7.80\times10^{-3}$ kg·m^2; inertia of vehicle, $I_{VE2} = 3.27$ kg·m^2; stiffness of Dual-mass flywheel (DMF), $k_f = 1.0$ kg·m/deg; stiffness of clutch with Single-mass flywheel (SMF), $k_C = 3.27$ kg·m/deg; stiffness of clutch with Dual-mass flywheel (DMF), $k_{fc} = 10000$ N·m/rad; stiffness of input shaft, $k_i = 10000$ N·m/rad; gear mesh stiffness, $k_g = 2.7\times10^8$ N/m; stiffness of drive shaft, $k_{VE2} = 6.63\times10^2$ N·m/rad; radius of engaged gear on input shaft, $R_{ie} = 35.5$ mm; radius of engaged gear on output shaft, $R_{oe} = 46.0$ mm; radius of unloaded gear on input shaft, $R_{iu} = 45.9$ mm; radius of unloaded gear on output shaft, $R_{ou} = 35.6$ mm. Here θ_i is the absolute displacement with the relevant subscripts (i=f,h,ie,ou,OG,$VE2$) of the sub-systems. The input torque $T_E(t)$ and drag torques are defined in the later section. The equations of motion based upon the LTI system model are derived as follows.

$$\underline{\underline{\mathbf{M}}}\ddot{\underline{\boldsymbol{\theta}}}(\mathbf{t})+\underline{\underline{\mathbf{K}}}\underline{\boldsymbol{\theta}}(\mathbf{t})=\underline{\mathbf{0}}. \tag{1}$$

$$\underline{\theta}=\begin{bmatrix}\theta_f & \theta_h & \theta_i & \theta_{ou} & \theta_{OG} & \theta_v\end{bmatrix}^{\mathrm{T}}. \tag{2}$$

$$\underline{\underline{\mathbf{M}}}=diag\begin{bmatrix}I_f, I_h, I_{ie}, I_{ou}, I_{OG}, I_{VE2}\end{bmatrix}. \tag{3}$$

$$\underline{\underline{\mathbf{K}}}=\begin{bmatrix} k_c & -k_c & 0 & 0 & 0 & 0 \\ -k_c & k_c+k_i & -k_i & 0 & 0 & 0 \\ 0 & -k_i & k_i+k_g\left(R_{iu}^2+R_{ie}^2\right) & k_gR_{iu}R_{ou} & k_gR_{ie}R_{oe} & 0 \\ 0 & 0 & k_gR_{iu}R_{ou} & k_gR_{ou}^2 & 0 & 0 \\ 0 & 0 & k_gR_{ie}R_{oe} & 0 & k_gR_{oe}^2+k_{VE2} & -k_{VE2} \\ 0 & 0 & 0 & 0 & -k_{VE2} & k_{VE2} \end{bmatrix}. \tag{4}$$

Table 1. Characteristics of the multi-staged clutch dampers (with SMF) and DMF.

Property		Stage	Clutch with SMF			DMF
			Type A	Type B	Type C	
Torsional stiffness, k_{Ci} (linearized in a piecewise manner) (kg·m/deg)		1	0.018	0.89	0.016	1.0
		2	0.11	1.52	0.05	-
		3	1.06	-	0.5	-
		4	3.27	-	1.01	-
Hysteresis, H_i (kg·m)		1	0.1	2.0	0.09	2.0
		2	0.2	2.7	0.1	-
		3	2.0	-	2.0	-
		4	2.7	-	2.7	-
Transition angle at positive side (δ_1 >0), ϕ_{pi} (degree)		1	3.0	0	6.0	27.0
		2	9.0	13.5	15.0	-
		3	17.0	-	15.0	-
		4	22.5	-	36.5	-
Transition angle at negative side (δ_1 >0), ϕ_{ni} (degree)		1	-2.0	-11.0	-5.0	-27.0
		2	-3.0	-14.0	-5.0	-
		3	-5.0	-	-15.0	-
		4	-8.5	-	-26.5	-
Preload	Magnitude of positive value	-	-	0.78	-	-
	Magnitude of negative value	-	-	-0.17	-	-
	Transition angle, ϕ_{Pr}	-	-	0	-	-

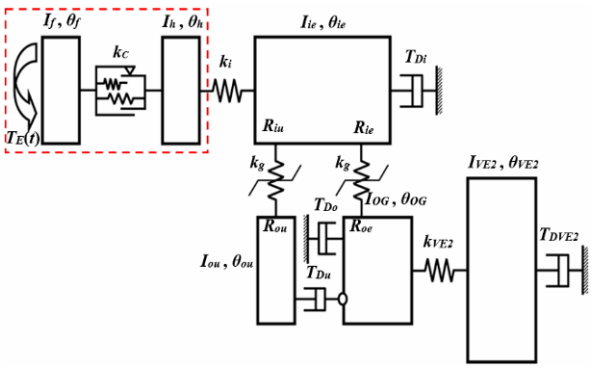

(a)

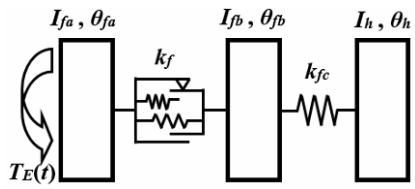

(b)

Fig. 1. 6DOF torsional system model for 3rd gear engaged and 5th gear unloaded case with Single-mass flywheel (SMF) and Dual-mass flywheel (DMF): (a) 6DOF system model with SMF; (b) schematic of Dual-mass flywheel (DMF).

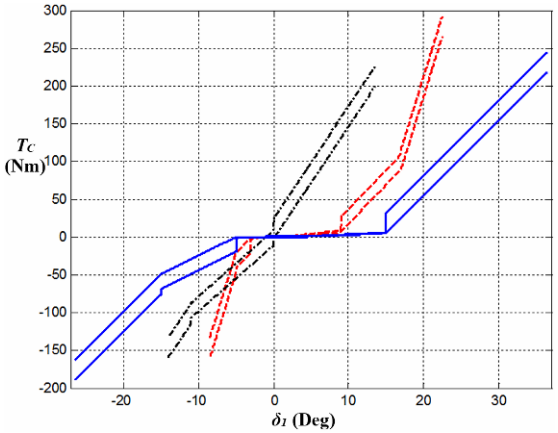

Fig. 2. Torque $T_C(\delta_1)$ profile for three clutch dampers based on the real-life clutch design. Key: – – –, clutch type A; – · –, clutch type B; ——, clutch type C.

In the prior studies [1-7], characteristics of gear rattle is defined by employing one specific clutch damper model. In general, the vehicle system has the multiple-staged clutch design concepts. Fig. 2 shows three real-life clutch models which are called as clutch types A, B and C given from the manufacturers. For example, clutch types A and B are narrow range of transition angles compared with a clutch type C. All of the clutch models have asymmetric transition angles and especially, the clutch type B includes a pre-load when the transition angle is changed from positive to negative side. Table 1 lists the employed properties for each clutch type as well as the Dual-mass flywheel (DMF). Also, vibro-impacts occur under several vehicle driving conditions. For instance, the driveline under the coast condition should fall into different dynamic conditions such as abrupt changes of input and effective drag torques. To simulate vibro-impacts in a gear pair, the 3rd gear engaged and 5th gear unloaded status will be discovered at 1800 RPM (for the WOT condition) and 3000 RPM (for both WOT and coast conditions), since the gear rattle in the manual transmission generally is observed in these ranges of engine operating conditions.

3. Nonlinear analysis of vibro-impacts with 6DOF system model

3.1 Nonlinear model of 6DOF torsional system and experimental results

Fig. 3 shows the schematic of 6DOF torsional system including nonlinear functions based upon the system illustrated in Fig. 1. The main nonlinearities concerned with this research are clutch torque $T_C(\delta_1)$, gear force on the engaged gear $F_{ge}(\rho_e)$, gear force on the unloaded gear $F_{gu}(\rho_u)$ and drag torques. Here, ρ_e and ρ_u are the relative displacements between engaged and unloaded gear pairs respectively. Drag torques are designated as follows: drag torque on the input shaft T_{Di}; drag torque on the output shaft T_{Do}; drag torque on the unloaded gear T_{Du}; drag torque on the vehicle T_{DVE2}. Here, δ_1 are the relative dis

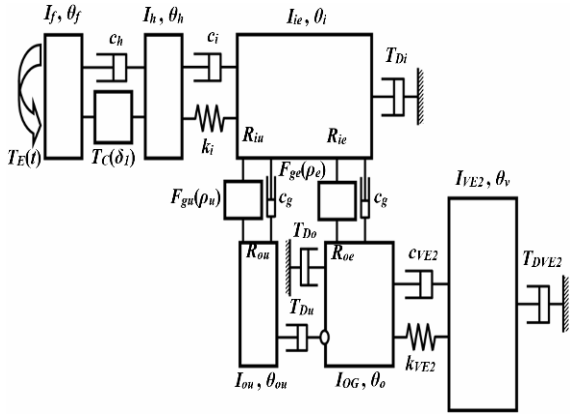

Fig. 3. Nonlinear model of the reduced order system for 3rd gear engaged and 5th gear unloaded case with the Single-mass flywheel (SMF) by including nonlinear functions.

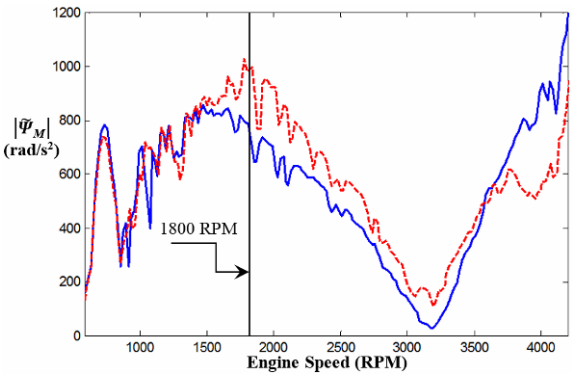

Fig. 4. Measured accelerations on the powertrain with the clutch type A under the WOT condition. Key: ——, acceleration measured on the engine; – – –, acceleration measured on the transmission.

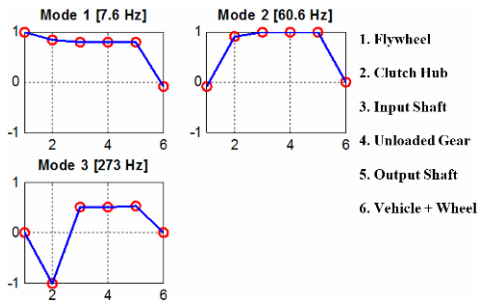

(a)

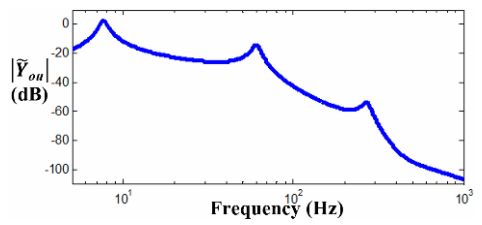

(b)

Fig. 5. Dynamic characteristics using linear time-invariant system model: (a) mode shapes of the 6DOF system; (b) mobility $\tilde{Y}_{ou}$ calculated at the unloaded gear.

placement between flywheel and clutch hub.

In general, the experimental data are given by the acceleration type measurement as shown in Fig. 4. This measured information is limited to the LTI system model which corresponds to the system illustrated in Fig. 1. Here, measured acceleration is designated as $\tilde{\Psi}_M$. As shown in Fig. 4, $\tilde{\Psi}_M$ of the transmission show the maximum value at 1800 RPM. Thus, the gear rattle of the system is assumed to be correlated with this firing frequency range which is defined as 60 Hz = 2×1800(RPM)/60(Min) since this system has a 4-stroke and 4-cylinder engine. Overall, the natural frequency of the vehicle system is assumed to be 60 Hz and it is incorporated with the gear rattling motions. Fig. 5 shows the simulated dynamic characteristics with LTI system model. When they are compared with the limited measured data shown in Fig. 4, the simulated natural frequencies and resonances are assumed to include the relevant natural frequency and its dynamic motions.

3.2 Investigation of multi-staged clutch dampers with asymmetric transition angles

The prior researches [1-7] have defined the mathematical model for the symmetric two-staged clutch dampers employed by the nonlinear torsional system shown in Fig. 3. In this study, this model can be developed further by including asymmetric transition angles and pre-load when the relative motion δ_1 (= $\theta_f - \theta_h$) on the clutch is changed from positive to negative side.

Here, θ_f and θ_h are defined as the absolute displacements of flywheel and clutch hub respectively. Fig. 6 shows the real-life clutch dampers with relevant component to be considered.

Fig. 6(a) illustrates the characteristics of clutch type B which contains asymmetric transition angles and pre-load. Fig. 6(b) illustrates the clutch torque induced by the stiffness T_S with the asymmetric transition angles designated as ϕ_{n1} and ϕ_{p1}. Here, ϕ_{n1} and ϕ_{p1} are defined as the transition angle on the negative and positive sides respectively. Figs. 6(c) and (d) shows the clutch torque T_H (or T_{SPr}) due to the hysteresis (or pre-load) where ϕ_{Pr} is the transition angle located at the pre-load. Also, T_{Pr1} and T_{Pr2} are the positive and negative pre-loads respectively.

Thus, the mathematical model for the general case of the multi-staged clutch dampers should include all the asymmetric cases as illustrated in Fig. 6.

First, consider two-staged clutch torque induced by stiffness as follows.

$$T_s(\delta_1)=\begin{cases} k_{C1}\phi_{p1}+k_{C2}(\delta_1-\phi_{p1}) & , \quad \delta_1>\phi_{p1} \\ k_{C1}\delta_1 & , \quad -\phi_{n1}<\delta_1<\phi_{p1} \\ -k_{C1}\phi_{n1}+k_{C2}(\delta_1+\phi_{n1}) & , \quad \delta_1<-\phi_{n1} \end{cases}. \tag{5}$$

where $T_S(\delta_1)$ is the function of δ_1. From Eq. (5), $T_S(\delta_1)$ is derived by using the hyperbolic tangent function *tanh* [6, 20, 30].

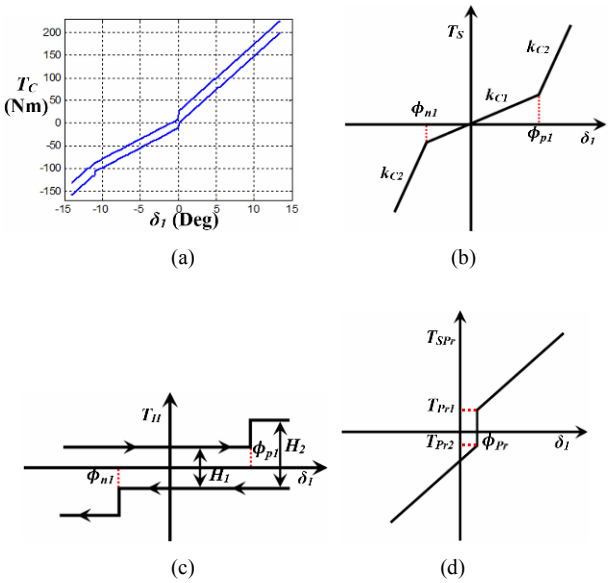

Fig. 6. Nonlinear characteristics of multi-staged clutch damper: (a) real-life multi-staged clutch damper; (b) clutch torque induced by stiffness with asymmetric transition angles; (c) clutch torque induced by hysteresis with asymmetric transition angles; (d) clutch torque induced by pre-load.

$$\begin{aligned} T_s(\delta_1) &= k_{C1}\delta_1 \\ &+\left[k_{C2}(\delta_1-\phi_{p1})+k_{C1}\phi_{p1}-k_{C1}\delta_1\right]\frac{1}{2}\left[\tanh\left\{\sigma_c(\delta_1-\phi_{p1})\right\}+1\right] \\ &+\left[k_{C2}(\delta_1+\phi_{n1})-k_{C1}\phi_{n1}-k_{C1}\delta_1\right]\frac{1}{2}\left[-\tanh\left\{\sigma_c(\delta_1+\phi_{n1})\right\}+1\right]. \end{aligned} \tag{6}$$

Here, σ_c is defined as the smoothening factor for the clutch torque [3, 6, 30]. Thus, Eq. (6) is summarized as follows.

$$\begin{aligned} T_s(\delta_1) &= k_{C1}\delta_1 \\ &+\frac{1}{2}(k_{C2}-k_{C1})(\delta_1-\phi_{p1})\left[\tanh\left\{\sigma_c(\delta_1-\phi_{p1})\right\}+1\right] \\ &-\frac{1}{2}(k_{C2}-k_{C1})(\delta_1+\phi_{n1})\left[\tanh\left\{\sigma_c(\delta_1+\phi_{n1})\right\}-1\right]. \end{aligned} \tag{7}$$

Second, develop three-staged clutch torque induced by stiffness as follows.

$$T_s(\delta_1)=\begin{cases} k_{C1}\phi_{p1}+k_{C2}(\phi_{p2}-\phi_{p1})+k_{C3}(\delta_1-\phi_{p2}) & , \quad \delta_1>\phi_{p2} \\ k_{C1}\phi_{p1}+k_{C2}(\delta_1-\phi_{p1}) & , \quad -\phi_{p1}<\delta_1<\phi_{p2} \\ k_{C1}\delta_1 & , \quad -\phi_{n1}<\delta_1<\phi_{p1} \\ -k_{C1}\phi_{n1}+k_{C2}(\delta_1+\phi_{n1}) & , \quad -\phi_{n2}<\delta_1<-\phi_{n1} \\ -k_{C1}\phi_{n1}-k_{C2}(\phi_{n2}-\phi_{n1})+k_{C3}(\delta_1+\phi_{n2}) & , \quad \delta_1<-\phi_{n2} \end{cases}. \tag{8}$$

From Eq. (8), $T_S(\delta_1)$ for three-staged clutch stiffness is derived using the hyperbolic tangent function *tanh* as well.

$$
\begin{aligned}
&T_s(\delta_1) = k_{C1}\delta_1 \\
&+\left[k_{C2}(\delta_1-\phi_{p1})+k_{C1}\phi_{p1}-k_{C1}\delta_1\right]\frac{1}{2}\left[\tanh\left\{\sigma_c(\delta_1-\phi_{p1})\right\}+1\right] \\
&+\left[k_{C3}(\delta_1-\phi_{p2})+k_{C2}(\phi_{p2}-\phi_{p1})+k_{C1}\phi_{p1}-k_{C2}(\delta_1-\phi_{p1})-k_{C1}\phi_{p1}\right] \\
&\cdot\frac{1}{2}\left[\tanh\left\{\sigma_c(\delta_1-\phi_{p2})\right\}+1\right] \\
&+\left[k_{C2}(\delta_1+\phi_{n1})-k_{C1}\phi_{n1}-k_{C1}\delta_1\right]\frac{1}{2}\left[-\tanh\left\{\sigma_c(\delta_1+\phi_{n1})\right\}+1\right] \\
&+\left[k_{C3}(\delta_1+\phi_{n2})-k_{C2}(\phi_{n2}-\phi_{n1})-k_{C1}\phi_{n1}-k_{C2}(\delta_1+\phi_{n1})+k_{C1}\phi_{n1}\right] \\
&\cdot\frac{1}{2}\left[-\tanh\left\{\sigma_c(\delta_1+\phi_{n2})\right\}+1\right]. \qquad (9)
\end{aligned}
$$

Likewise, Eq. (9) is summarized as follows.

$$
\begin{aligned}
&T_s(\delta_1) = k_{C1}\delta_1 \\
&+\frac{1}{2}(k_{C3}-k_{C2})(\delta_1-\phi_{p2})\left[\tanh\left\{\sigma_c(\delta_1-\phi_{p2})\right\}+1\right] \\
&+\frac{1}{2}(k_{C2}-k_{C1})(\delta_1-\phi_{p1})\left[\tanh\left\{\sigma_c(\delta_1-\phi_{p1})\right\}+1\right] \\
&-\frac{1}{2}(k_{C3}-k_{C2})(\delta_1+\phi_{n2})\left[\tanh\left\{\sigma_c(\delta_1+\phi_{n2})\right\}-1\right] \\
&-\frac{1}{2}(k_{C2}-k_{C1})(\delta_1+\phi_{n1})\left[\tanh\left\{\sigma_c(\delta_1+\phi_{n1})\right\}-1\right]. \qquad (10)
\end{aligned}
$$

Finally, $T_S(\delta_1)$ for the multi-staged clutch with asymmetric transition angles are derived based upon Eqs. (5)-(10).

$$
\begin{aligned}
&T_s(\delta_1) = k_{C1}\delta_1 \\
&+\frac{1}{2}\left(k_{C(N)}-k_{C(N-1)}\right)\left(\delta_1-\phi_{p(N-1)}\right)\left[\tanh\left\{\sigma_c\left(\delta_1-\phi_{p(N-1)}\right)\right\}+1\right] \\
&+\frac{1}{2}\left(k_{C(N-1)}-k_{C(N-2)}\right)\left(\delta_1-\phi_{p(N-2)}\right)\left[\tanh\left\{\sigma_c\left(\delta_1-\phi_{p(N-2)}\right)\right\}+1\right] \\
&+\cdots \\
&+\frac{1}{2}(k_{C3}-k_{C2})(\delta_1-\phi_{p2})\left[\tanh\left\{\sigma_c(\delta_1-\phi_{p2})\right\}+1\right] \\
&+\frac{1}{2}(k_{C2}-k_{C1})(\delta_1-\phi_{p1})\left[\tanh\left\{\sigma_c(\delta_1-\phi_{p1})\right\}+1\right] \\
&-\frac{1}{2}\left(k_{C(N)}-k_{C(N-1)}\right)\left(\delta_1+\phi_{n(N-1)}\right)\left[\tanh\left\{\sigma_c\left(\delta_1+\phi_{n(N-1)}\right)\right\}-1\right] \\
&-\frac{1}{2}\left(k_{C(N-1)}-k_{C(N-2)}\right)\left(\delta_1+\phi_{n(N-2)}\right)\left[\tanh\left\{\sigma_c\left(\delta_1+\phi_{n(N-2)}\right)\right\}-1\right] \\
&-\cdots \\
&-\frac{1}{2}(k_{C3}-k_{C2})(\delta_1+\phi_{n2})\left[\tanh\left\{\sigma_c(\delta_1+\phi_{n2})\right\}-1\right] \\
&-\frac{1}{2}(k_{C2}-k_{C1})(\delta_1+\phi_{n1})\left[\tanh\left\{\sigma_c(\delta_1+\phi_{n1})\right\}-1\right]. \qquad (11)
\end{aligned}
$$

$$
T_s(\delta_1) = k_{C1}\delta_1 + \frac{1}{2}\sum_{i=2}^{N}\left(k_{C(i)}-k_{C(i-1)}\right)\left(T_{sp(i-1)}-T_{sn(i-1)}\right), \qquad (12a)
$$

$$
T_{sp(i)} = \left(\delta_1-\phi_{p(i)}\right)\left[\tanh\left\{\sigma_c\left(\delta_1-\phi_{p(i)}\right)\right\}+1\right], \qquad (12b)
$$

$$
T_{sn(i)} = \left(\delta_1+\phi_{n(i)}\right)\left[\tanh\left\{\sigma_c\left(\delta_1+\phi_{n(i)}\right)\right\}-1\right]. \qquad (12c)
$$

As a next step, the clutch torque induced by hysteresis T_H should be considered as shown in Fig. 6(c). First, if the system has only one stage, T_H has simple formulation.

$$
T_H\left(\delta_1,\dot{\delta}_1\right) = \frac{H_1}{2}\tanh\left(\sigma_c\dot{\delta}_1\right). \qquad (13)
$$

where $T_H\left(\delta_1,\dot{\delta}_1\right)$ is the function of δ_1 and $\dot{\delta}_1$. Second, T_H for two-staged clutch is derived based upon the illustration in Fig. 6(c).

$$
\begin{aligned}
&T_H\left(\delta_1,\dot{\delta}_1\right) = \frac{H_1}{2}\tanh\left(\sigma_c\dot{\delta}_1\right) \\
&+\frac{1}{2}\left[\left(\frac{H_2}{2}-\frac{H_1}{2}\right)+\frac{H_2}{2}\tanh\left(\sigma_c\dot{\delta}_1\right)-\frac{H_1}{2}\tanh\left(\sigma_c\dot{\delta}_1\right)\right] \\
&\cdot\left[\tanh\left\{\sigma_c(\delta_1-\phi_{p1})\right\}+1\right] \qquad (14) \\
&+\frac{1}{2}\left[-\left(\frac{H_2}{2}-\frac{H_1}{2}\right)+\frac{H_2}{2}\tanh\left(\sigma_c\dot{\delta}_1\right)-\frac{H_1}{2}\tanh\left(\sigma_c\dot{\delta}_1\right)\right] \\
&\cdot\left[-\tanh\left\{\sigma_c(\delta_1+\phi_{n1})\right\}+1\right].
\end{aligned}
$$

$$
\begin{aligned}
&T_H\left(\delta_1,\dot{\delta}_1\right) = \frac{H_2}{2}\tanh\left(\sigma_c\dot{\delta}_1\right) \\
&+\left(\frac{H_2}{4}-\frac{H_1}{4}\right)\tanh\left\{\sigma_c(\delta_1-\phi_{p1})\right\}\left[1+\tanh\left(\sigma_c\dot{\delta}_1\right)\right] \qquad (15) \\
&+\left(\frac{H_2}{4}-\frac{H_1}{4}\right)\tanh\left\{\sigma_c(\delta_1+\phi_{n1})\right\}\left[1-\tanh\left(\sigma_c\dot{\delta}_1\right)\right].
\end{aligned}
$$

Third, T_H for three-staged clutch is derived with the similar manner.

$$
\begin{aligned}
&T_H\left(\delta_1,\dot{\delta}_1\right) = \frac{H_1}{2}\tanh\left(\sigma_c\dot{\delta}_1\right) \\
&+\frac{1}{2}\left[\left(\frac{H_2}{2}-\frac{H_1}{2}\right)+\left(\frac{H_2}{2}-\frac{H_1}{2}\right)\tanh\left(\sigma_c\dot{\delta}_1\right)\right] \\
&\cdot\left[\tanh\left\{\sigma_c(\delta_1-\phi_{p1})\right\}+1\right] \\
&+\frac{1}{2}\left[-\left(\frac{H_2}{2}-\frac{H_1}{2}\right)+\left(\frac{H_2}{2}-\frac{H_1}{2}\right)\tanh\left(\sigma_c\dot{\delta}_1\right)\right] \\
&\cdot\left[-\tanh\left\{\sigma_c(\delta_1+\phi_{n1})\right\}+1\right] \\
&+\frac{1}{2}\left[\left(\frac{H_3}{2}-\frac{H_2}{2}\right)+\left(\frac{H_3}{2}-\frac{H_2}{2}\right)\tanh\left(\sigma_c\dot{\delta}_1\right)\right] \\
&\cdot\left[\tanh\left\{\sigma_c(\delta_1-\phi_{p2})\right\}+1\right]
\end{aligned}
$$

$$+\frac{1}{2}\left[-\left(\frac{H_3}{2}-\frac{H_2}{2}\right)+\left(\frac{H_3}{2}-\frac{H_2}{2}\right)\tanh\left(\sigma_c\dot{\delta}_1\right)\right]$$
$$\cdot\left[-\tanh\left\{\sigma_c\left(\delta_1+\phi_{n2}\right)\right\}+1\right]. \quad (16)$$

$$T_H\left(\delta_1,\dot{\delta}_1\right)=\frac{H_3}{2}\tanh\left(\sigma_c\dot{\delta}_1\right)$$
$$+\left(\frac{H_2}{4}-\frac{H_1}{4}\right)\tanh\left\{\sigma_c\left(\delta_1-\phi_{p1}\right)\right\}\left[1+\tanh\left(\sigma_c\dot{\delta}_1\right)\right]$$
$$+\left(\frac{H_2}{4}-\frac{H_1}{4}\right)\tanh\left\{\sigma_c\left(\delta_1+\phi_{n1}\right)\right\}\left[1-\tanh\left(\sigma_c\dot{\delta}_1\right)\right]$$
$$+\left(\frac{H_3}{4}-\frac{H_2}{4}\right)\tanh\left\{\sigma_c\left(\delta_1-\phi_{p2}\right)\right\}\left[1+\tanh\left(\sigma_c\dot{\delta}_1\right)\right]$$
$$+\left(\frac{H_3}{4}-\frac{H_2}{4}\right)\tanh\left\{\sigma_c\left(\delta_1+\phi_{n2}\right)\right\}\left[1-\tanh\left(\sigma_c\dot{\delta}_1\right)\right]. \quad (17)$$

Finally, T_H for the multi-staged clutch case with asymmetric transition angles is derived from Eqs. (13)-(17).

$$T_H\left(\delta_1,\dot{\delta}_1\right)=\frac{H_{(N)}}{2}\tanh\left(\sigma_c\dot{\delta}_1\right)$$
$$+\left(\frac{H_{(N)}}{4}-\frac{H_{(N-1)}}{4}\right)\left[\tanh\left\{\sigma_c\left(\delta_1-\phi_{p(N-1)}\right)\right\}\left[1+\tanh\left(\sigma_c\dot{\delta}_1\right)\right]\right.$$
$$\left.+\tanh\left\{\sigma_c\left(\delta_1+\phi_{n(N-1)}\right)\right\}\left[1-\tanh\left(\sigma_c\dot{\delta}_1\right)\right]\right]$$
$$+\left(\frac{H_{(N-1)}}{4}-\frac{H_{(N-2)}}{4}\right)\left[\tanh\left\{\sigma_c\left(\delta_1-\phi_{p(N-2)}\right)\right\}\left[1+\tanh\left(\sigma_c\dot{\delta}_1\right)\right]\right.$$
$$\left.+\tanh\left\{\sigma_c\left(\delta_1+\phi_{n(N-2)}\right)\right\}\left[1-\tanh\left(\sigma_c\dot{\delta}_1\right)\right]\right]$$
$$+\cdots$$
$$+\left(\frac{H_3}{4}-\frac{H_2}{4}\right)\left[\tanh\left\{\sigma_c\left(\delta_1-\phi_{p2}\right)\right\}\left[1+\tanh\left(\sigma_c\dot{\delta}_1\right)\right]\right.$$
$$\left.+\tanh\left\{\sigma_c\left(\delta_1+\phi_{n2}\right)\right\}\left[1-\tanh\left(\sigma_c\dot{\delta}_1\right)\right]\right]+\left(\frac{H_2}{4}-\frac{H_1}{4}\right)$$
$$\left[\tanh\left\{\sigma_c\left(\delta_1-\phi_{p1}\right)\right\}\left[1+\tanh\left(\sigma_c\dot{\delta}_1\right)\right]\right.$$
$$\left.+\tanh\left\{\sigma_c\left(\delta_1+\phi_{n1}\right)\right\}\left[1-\tanh\left(\sigma_c\dot{\delta}_1\right)\right]\right]. \quad (18)$$

$$T_H\left(\delta_1,\dot{\delta}_1\right)=\frac{H_{(N)}}{2}\tanh\left(\sigma_c\dot{\delta}_1\right)$$
$$+\sum_{i=2}^{N}\left(\frac{H_{(i)}}{4}-\frac{H_{(i-1)}}{4}\right)\left(T_{Hp(i-1)}-T_{Hn(i-1)}\right), \quad (19a)$$
$$T_{Hp(i)}\tanh\left\{\sigma_c\left(\delta_1-\phi_{p(i)}\right)\right\}\left[1+\tanh\left(\sigma_c\dot{\delta}_1\right)\right], \quad (19b)$$
$$T_{Hn(i)}\tanh\left\{\sigma_c\left(\delta_1+\phi_{n(i)}\right)\right\}\left[1-\tanh\left(\sigma_c\dot{\delta}_1\right)\right]. \quad (19c)$$

In order to include the pre-load effect as illustrated in Fig. 6(d), δ_1 is first modified by $\delta_{1\mathrm{pr}}=\delta_1-\phi_{\mathrm{Pr}}$. Then, the pre-load T_{Pr} is calculated by the function of $\delta_{1\mathrm{pr}}$.

$$T_{\mathrm{SPr}}\left(\delta_{1\mathrm{pr}}\right)=\frac{1}{2}T_{\mathrm{Pr1}}\left[\tanh\left(\sigma_c\delta_{1\mathrm{pr}}\right)+1\right]$$
$$+\frac{1}{2}T_{\mathrm{Pr2}}\left[-\tanh\left(\sigma_c\delta_{1\mathrm{pr}}\right)+1\right]. \quad (20)$$

Thus, when the clutch torque is affected by the pre-load, the relative displacement δ_1 should be modified by $\delta_{1\mathrm{pr}}=\delta_1-\phi_{\mathrm{Pr}}$ along with Eqs. (5)-(19). Overall, the total clutch torque by including all the effect as illustrated in Fig. 6 is calculated as follows.

$$T_C\left(\delta_{1\mathrm{pr}},\dot{\delta}_{1\mathrm{pr}}\right)=T_S\left(\delta_{1\mathrm{pr}}\right)+T_H\left(\delta_{1\mathrm{pr}},\dot{\delta}_{1\mathrm{pr}}\right)+T_{\mathrm{SPr}}\left(\delta_{1\mathrm{pr}}\right). \quad (21)$$

In this study, 1×10^3 is employed as a value of smoothening factor σ_c.

3.3 Nonlinear models for the numerical analysis under the WOT condition

Again, the nonlinear equations in terms of the relative displacement $\underline{\boldsymbol{\delta}}(t)$ can be derived as follows. First, the state vector of absolute displacement $\underline{\mathbf{x}}(t)$ is:

$$\underline{\mathbf{x}}(t)=\left[\theta_f\ \theta_h\ \theta_i\ \theta_{ou}\ \theta_o\ \theta_{VE2}\ \dot{\theta}_f\ \dot{\theta}_h\ \dot{\theta}_i\ \dot{\theta}_{ou}\ \dot{\theta}_o\ \dot{\theta}_{VE2}\right]^{\mathrm{T}}. \quad (22)$$

Thus, the state space model using state matrix $\underline{\underline{\mathbf{S}}}$, nonlinear function vector $\underline{\mathbf{T}_{\mathbf{non}}}(t)$ and input torque vector $\underline{\mathbf{T}_{\mathbf{E}}}(t)$ are defined as follows.

$$\dot{\underline{\mathbf{x}}}(t)=\underline{\underline{\mathbf{S}}}\,\underline{\mathbf{x}}(t)+\underline{\mathbf{T}_{\mathbf{non}}}(t)+\underline{\mathbf{T}_{\mathbf{E}}}(t). \quad (23)$$

$$\underline{\underline{\mathbf{S}}}=\begin{bmatrix}\underline{\underline{\mathbf{0}}} & \underline{\underline{\mathbf{I}}}\\ \underline{\underline{\mathbf{K_s}}} & \underline{\underline{\mathbf{C_s}}}\end{bmatrix}, \quad (24a)$$

$$\underline{\underline{\mathbf{K_s}}}=\begin{bmatrix}0&0&0&0&0&0\\0&-k_i/I_h&k_i/I_h&0&0&0\\0&k_i/I_{ie}&-k_i/I_{ie}&0&0&0\\0&0&0&0&0&0\\0&0&0&0&-k_{VE2}/I_{OG}&k_{VE2}/I_{OG}\\0&0&0&0&k_{VE2}/I_{VE2}&-k_{VE2}/I_{VE2}\end{bmatrix},$$

$$\underline{\underline{\mathbf{C_s}}}=\begin{bmatrix}-c_h/I_f&c_h/I_h&0&0&0&0\\c_h/I_h&-(c_h+c_i)/I_h&c_i/I_h&0&0&0\\0&c_i/I_{ie}&-\left(c_i+c_{ge}R_{ie}^2+c_{gu}R_{iu}^2\right)/I_{ie}&-c_{gu}R_{iu}R_{ou}/I_{ie}&-c_{ge}R_{ie}R_{oe}/I_{ie}&0\\0&0&-c_{gu}R_{iu}R_{ou}/I_{ou}&-c_{gu}R_{ou}^2/I_{ou}&0&0\\0&0&-c_{ge}R_{ie}R_{oe}/I_{OG}&0&-\left(c_{ge}R_{oe}^2+c_{VE2}\right)/I_{OG}&c_{VE2}/I_{OG}\\0&0&0&0&c_{VE2}/I_{VE2}&-c_{VE2}/I_{VE2}\end{bmatrix}, \quad (24b,c)$$

$$\underline{\mathbf{T_E}}(t)=\begin{bmatrix}0\\0\\0\\0\\0\\0\\T_E(t)/I_f\\0\\0\\0\\0\end{bmatrix},\quad \underline{\mathbf{T_{non}}}(t)=\begin{bmatrix}0\\0\\0\\0\\0\\0\\-T_C\left(\delta_{Ipr},\dot{\delta}_{Ipr}\right)/I_f\\T_C\left(\delta_{Ipr},\dot{\delta}_{Ipr}\right)/I_h\\-\left[R_{iu}F_{gu}(\rho_u)+R_{ie}F_{ge}(\rho_e)+T_{Di}\right]/I_{ie}\\\left[-R_{ou}F_{gu}(\rho_u)+T_{Du}\right]/I_{ou}\\\left[-R_{oe}F_{ge}(\rho_e)+T_{Do}+T_{Du}\right]/I_{OG}\\-T_{DVE2}/I_{VE2}\end{bmatrix}, \tag{24d,e}$$

$$\rho_e=R_{ie}\theta_i+R_{oe}\theta_o,\quad \rho_u=R_{iu}\theta_i+R_{ou}\theta_o. \tag{24f,g}$$

$$F_{gi}=k_g\rho_i+k_g\frac{\left(\rho_i-\frac{b}{2}\right)\tanh\left\{\sigma_g\left(\rho_i-\frac{b}{2}\right)\right\}-\left(\rho_i+\frac{b}{2}\right)\tanh\left\{\sigma_g\left(\rho_i+\frac{b}{2}\right)\right\}}{2}, \tag{24h,i}$$

($i = e$ or u).

Here, subscript e (or u) is defined as the engaged (or unloaded) gear and 1×10^{10} is employed as a value of smoothening factor σ_g. Gear backlash is designated as b employed by 0.1mm in the simulation. Also, $\mathbf{K_s}$ and $\mathbf{C_s}$ are the normalized stiffness and damping matrices respectively. Damping values are defined as follows: damping of the clutch hub, c_h; damping of the input shaft, c_i; damping of engaged gear pair, c_{ge}; damping of unloaded gear pair, c_{gu}; damping of the drive shaft, c_{VE2}. These values are assumed by using the modal damping matrix [6]. Then, the state vector $\underline{\boldsymbol{\delta}}(t)$ is defined as follows.

$$\underline{\boldsymbol{\delta}}(t)=\left[\delta_1(t)\quad \delta_2(t)\quad \delta_3(t)\quad \delta_4(t)\quad \delta_5(t)\right], \tag{25a}$$

$$\delta_1(t)=\theta_f(t)-\theta_h(t),\quad \delta_2(t)=\theta_h(t)-\theta_i(t), \tag{25b,c}$$

$$\delta_3(t)=R_{ie}\theta_i(t)+R_{oe}\theta_o(t), \tag{25d}$$

$$\delta_4(t)=R_{iu}\theta_i(t)+R_{ou}\theta_u(t), \tag{25e}$$

$$\delta_5(t)=\theta_o(t)-\theta_{VE2}(t). \tag{25f}$$

Thus, the state vector $\underline{\mathbf{x}_\mathbf{r}}(t)$ for the relative motions is derived by using the transformation matrix $\underline{\underline{\mathbf{P}}}$.

$$\underline{\mathbf{x}_\mathbf{r}}(t)=\left[\delta_1\ \delta_2\ \delta_3\ \delta_4\ \delta_5\ \dot{\delta}_1\ \dot{\delta}_2\ \dot{\delta}_3\ \dot{\delta}_4\ \dot{\delta}_5\right]^{\mathrm{T}}, \tag{26a}$$

$$\underline{\mathbf{x}_\mathbf{r}}(t)=\underline{\underline{\mathbf{P}_\mathbf{r}}}\,\underline{\mathbf{x}}(t),\quad \underline{\underline{\mathbf{P}_\mathbf{r}}}=\begin{bmatrix}\underline{\underline{\mathbf{P}}} & \underline{\underline{\mathbf{0}}}\\ \underline{\underline{\mathbf{0}}} & \underline{\underline{\mathbf{P}}}\end{bmatrix}, \tag{26b,c}$$

$$\underline{\underline{\mathbf{P}}}=\begin{bmatrix}1 & -1 & 0 & 0 & 0 & 0\\ 0 & 1 & -1 & 0 & 0 & 0\\ 0 & 0 & R_{ie} & 0 & R_{oe} & 0\\ 0 & 0 & R_{iu} & R_{ou} & 0 & 0\\ 0 & 0 & 0 & 0 & 1 & -1\end{bmatrix}. \tag{26d}$$

Table 2. Engine torque profiles with idling (at 700 RPM) and WOT (at 1800 and 3000 RPM) conditions.

Property			Engine speed (RPM)		
			700	1800	3000
Magnitude (Nm)	Mean component	T_M	22.0	168.9	192.32
	Alternating component	T_{p1}	41.5	251.5	589.6
		T_{p2}	14.4	106.9	143.3
		T_{p3}	4.3	29.8	53.3
		T_{p4}	2.7	24.2	24.2
		T_{p5}	1.8	18.0	14.1
Phase (rad)	Alternating component	ϕ_{p1}	-1.90	-1.93	-1.71
		ϕ_{p2}	-2.69	-2.58	-2.37
		ϕ_{p3}	2.25	2.16	3.14
		ϕ_{p4}	0.64	0.72	2.18
		ϕ_{p5}	-0.38	-0.09	1.40

The relationship between $\underline{\mathbf{x}}(t)$ and $\underline{\mathbf{x}_\mathbf{r}}(t)$ are defined with respect to Eqs. (23) and (24).

$$\underline{\mathbf{x}}(t)=\underline{\underline{\mathbf{P}_\mathbf{r}^+}}\,\underline{\mathbf{x}_\mathbf{r}}(t),\quad \underline{\underline{\mathbf{P}_\mathbf{r}^+}}=\left(\underline{\underline{\mathbf{P}_\mathbf{r}^{\mathbf{T}}}}\,\underline{\underline{\mathbf{P}_\mathbf{r}}}\right)^{-1}\underline{\underline{\mathbf{P}_\mathbf{r}^{\mathbf{T}}}}. \tag{27a,b}$$

Here, pseudo inverse matrix $\underline{\underline{\mathbf{P}_\mathbf{r}^+}}$ is used for $n\times m$ ($n \neq m$) matrix $\underline{\underline{\mathbf{P}_\mathbf{r}}}$. Thus, this article will examine the relative motions in terms of $\underline{\mathbf{x}_\mathbf{r}}(t)$ by using the relationship as follows.

$$\dot{\underline{\mathbf{x}}}_\mathbf{r}(t)=\underline{\underline{\mathbf{S}^*}}\,\underline{\mathbf{x}_\mathbf{r}}(t)+\underline{\mathbf{T}^*_{\mathbf{non}}}(t)+\underline{\mathbf{T}^*_{\mathbf{E}}}(t), \tag{28a}$$

$$\underline{\underline{\mathbf{S}^*}}=\underline{\underline{\mathbf{P}_\mathbf{r}}}\,\underline{\underline{\mathbf{S}}}\,\underline{\underline{\mathbf{P}_\mathbf{r}^+}},\quad \underline{\mathbf{T}^*_{\mathbf{non}}}(t)=\underline{\underline{\mathbf{P}_\mathbf{r}}}\,\underline{\mathbf{T}_{\mathbf{non}}}(t), \tag{28b,c}$$

$$\underline{\mathbf{T}^*_{\mathbf{E}}}(t)=\underline{\underline{\mathbf{P}_\mathbf{r}}}\,\underline{\mathbf{T}_{\mathbf{E}}}(t). \tag{28d}$$

In this study, the modified Runge-Kutta method suggested by Dormand and Prince is used to investigate the dynamic characteristics of gear rattle [31]. The employed input torque $T_E(t)$ includes the mean and alternating components as follows.

$$T_E(t)=T_M+\sum_{i=1}^{n}T_{pi}\cos\left(i\Omega_p t+\phi_{pi}\right). \tag{29}$$

Here, T_{pi} is the amplitude of alternating parts at i^{th} harmonic, ϕ_{pi} is the phase at i^{th} harmonic and Ω_p is the firing frequency. Table 2 lists the engine torque profiles along with different engine speeds. For example, the engine torque profiles for 700 RPM shows the mean and alternating components under the idling condition. Each components listed in 1800 and 3000 RPM is measured under the WOT condition. Table 3 describes the employed properties under 1800 and 3000 RPM by assuming that the viscous dampings associated with each lumped system are same as each other (designated as "c")

Table 3. Employed properties for the drag torques along with different engine speeds.

Drag toque (Nm)	Engine speed	
	1800 RPM	3000 RPM
Drag toque on the input shaft, T_{Di}	13.3	26.9
Drag toque on the input shaft, T_{Di}	10.3	20.7
Drag toque on the unloaded gear, T_{Du}	1.38	2.8
Drag toque on the vehicle, T_{DVE2}	189.0	189.0

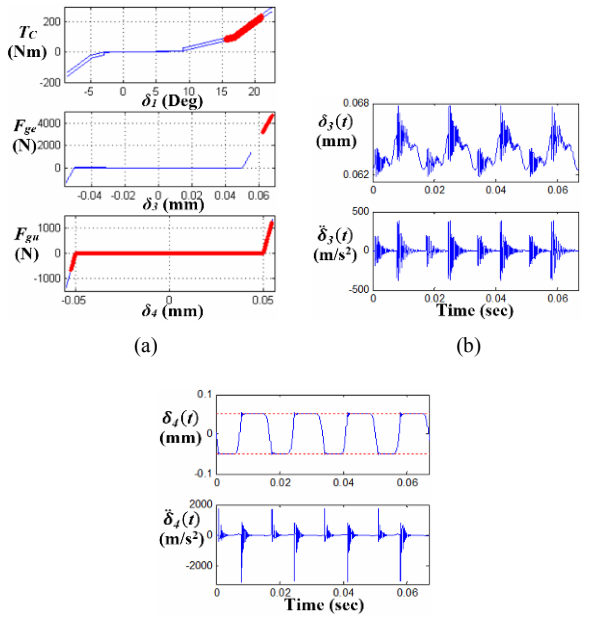

Fig. 7. Clutch torque (or gear mesh forces) and relative displacement with the clutch type A under the WOT condition at 1800 RPM: (a) clutch torque (or gear forces) vs. relative displacement; (b) relative motions of the engaged gear pair; (c) relative motions of the unloaded gear pair.

except for the damping on the unloaded gear (let *"0.2c"*).

3.4 Numerical results along with different clutch dampers and engine speed

Figs. 7-10 show the numerical results in terms of clutch torque (or gear forces) vs. relative displacement and relative motions of the engaged (or unloaded) gear pair in the time domain. Here, both ends of gear backlash *b*/2 and –*b*/2 are marked by red dotted lines. In this research, the gear rattle is examined along with different clutch dampers as well as different engine speeds. First, vibro-impacts on the gear pair are dependent upon the different clutch design concepts as shown in Figs. 7-9.

For example, severe vibro-impact is observed in the unloaded gear pair on the clutch type A. As shown in Figs. 7(a) and (c), "double-sided" impact is seen on the unloaded gear pair [6, 20]. Also, the simulated peak-to-peak (P-P) accelerations on both engaged and unloaded gear pairs are much higher than P-P accelerations for the other clutch dampers as shown in Figs. 8 and 9. Table 4 compares the P-P accelera-

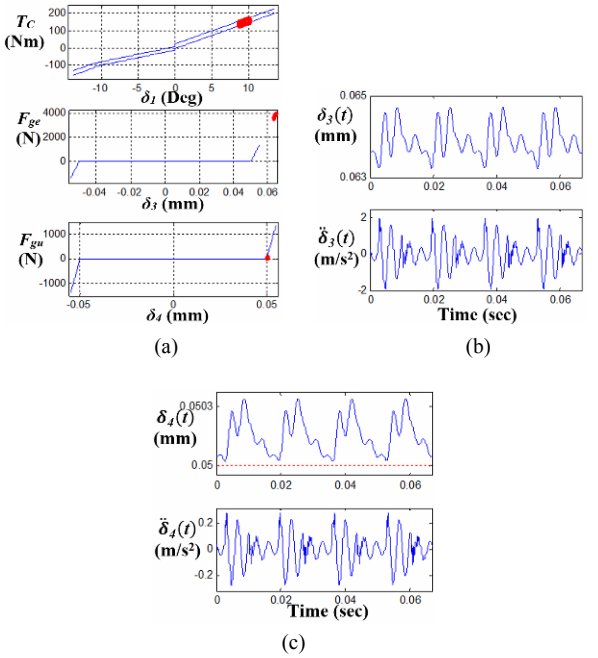

Fig. 8. Clutch torque (or gear mesh forces) and relative displacement with the clutch type B under the WOT condition at 1800 RPM: (a) clutch torque (or gear forces) vs. relative displacement; (b) relative motions of the engaged gear pair; (c) relative motions of the unloaded gear pair.

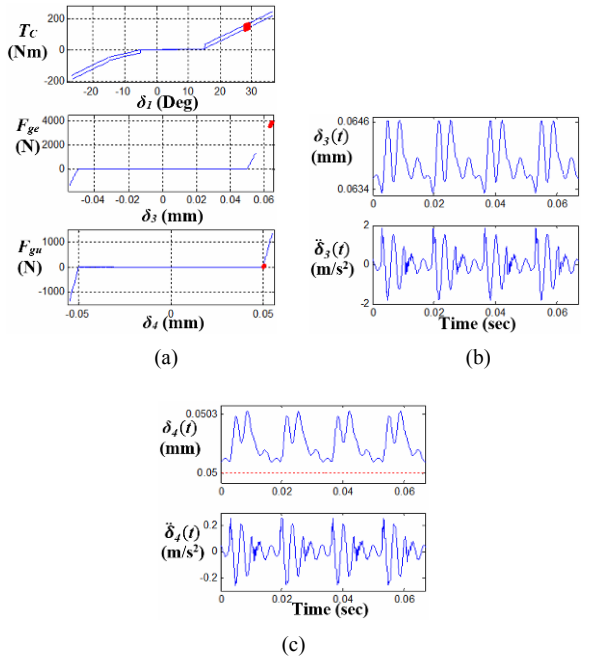

Fig. 9. Clutch torque (or gear mesh forces) and relative displacement with the clutch type C under the WOT condition at 1800 RPM: (a) clutch torque (or gear forces) vs. relative displacement; (b) relative motions of the engaged gear pair; (c) relative motions of the unloaded gear pair.

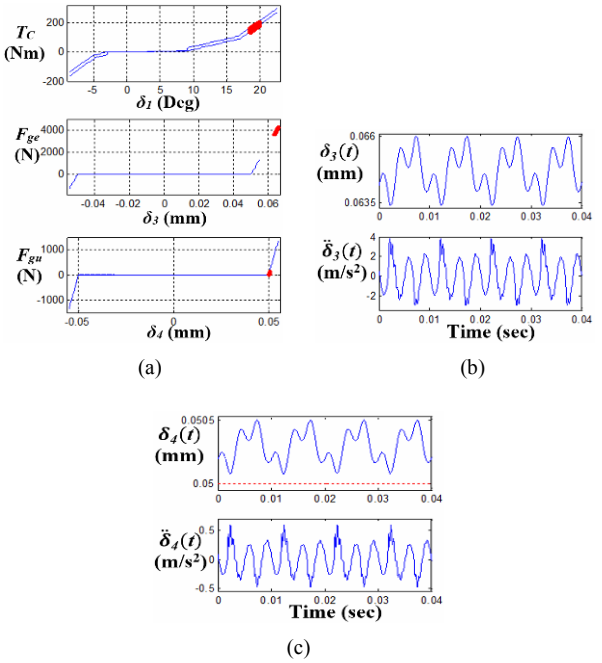

Fig. 10. Clutch torque (or gear mesh forces) and relative displacement with the clutch type A under the WOT condition at 3000 RPM: (a) clutch torque (or gear forces) vs. relative displacement; (b) relative motions of the engaged gear pair; (c) relative motions of the unloaded gear pair.

tions of the clutch type A with the clutch types B and C. The P-P accelerations with the clutch type A are 769.5 m/s^2 and 4845.0 m/s^2 for the engaged and unloaded gear pairs respectively. On the other hand, the P-P accelerations with the clutch types B and C are less than 4.0 m/s^2 and 0.6 m/s^2 for the engaged and unloaded gear pairs respectively. Second, P-P accelerations under 3000 RPM for all the clutch types show the rattle-free conditions defined as "no-impact". This indicates that vibro-impacts are dependent upon the engine speed as well. Third, when the vibro-impacts on the clutch type A are examined with two different engine speeds (1800 and 3000 RPM), their behaviors are clearly different with respect to the dynamic clutch torque T_C. For example, T_C at 1800 RPM pass through the pre-load regime between 3rd and 4th stiffness values as shown in Fig. 7. However, T_C at 3000 RPM is not located at the pre-load regime as seen in Fig. 10(a). Thus, vibro-impacts are expected to occur when T_C is located between the pre-load or stiffness changing regimes.

When the clutch types B and C are examined, there is no dynamic torque exhibiting between different stiffnesses or under the pre-load regime.

4. Examination of the coast condition

4.1 Linear analysis based upon the experimental results

Fig. 11 shows the measured accelerations on the engine and transmission. When these measurements are compared with the data shown in Fig. 4, the dynamic characteristics of the

Table 4. Simulated peak-to-peak accelerations for each clutch type under the WOT condition along with two different engine speeds.

Engine speed (RPM)	Peak-to-peak acceleration	Clutch type		
		A	B	C
1800	Engaged gear (m/s^2)	769.5	3.93	3.68
	Unloaded gear (m/s^2)	4845.0	0.56	0.52
	Impact type	Double-sided impact	No-impact	No-impact
300	Engaged gear (m/s^2)	6.80	5.30	4.96
	Unloaded gear (m/s^2)	1.07	0.83	0.77
	Impact type	No-impact	No-impact	No-impact

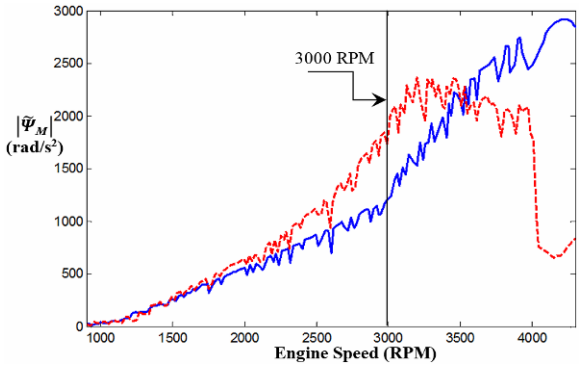

Fig. 11. Measured accelerations on the powertrain with the clutch type A under the coast condition. Key: ——, acceleration measured on the engine; - - - -, acceleration measured on the transmission.

acceleration under the coast condition are different. First, the maximum values of acceleration (assumed as resonance) under the WOT condition is moved into the higher range of engine speed between 3000 to 3500 RPM. Second, the dynamic characteristic of the engine acceleration is also changed compared with the data shown in Fig. 4 since there is no tip-in of the acceleration pedal under the coast condition.

Thus, from the given measured data, the system characteristics based upon the Linear time-invariant (LTI) system can be evaluated. In this study, the coast condition will be investigated with focus on the 3000 RPM (= 100 Hz, firing frequency) as indicated in Fig. 11.

Based upon the measured data under the coast condition, the effective property of the mode and natural frequency can be evaluated by assuming that the system is still affected by the clutch spring mode. Thus, the effective clutch stiffness values can be anticipated with respect to 100 Hz of the natural frequency. Fig. 12 show the dynamic characteristics simulated with LTI system model by increasing the default clutch stiffness value 3.27 kg·m/deg up to 4 times. When the results are compared with the system characteristics shown in Fig. 5, the mode shapes are almost same as each other except for the

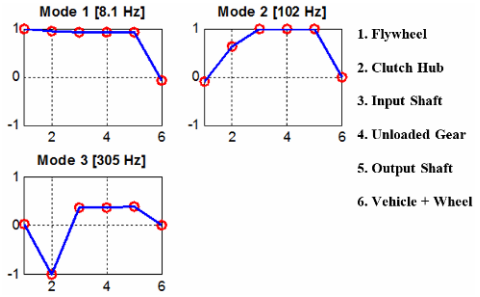

(a)

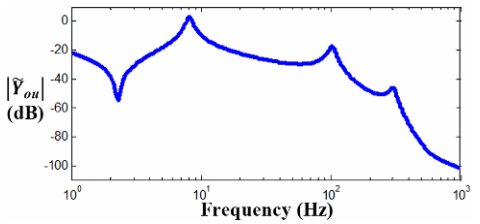

(b)

Fig. 12. Dynamic characteristics using linear time-invariant system model under the coast condition: (a) mode shapes of the 6DOF system; (b) mobility $\tilde{Y}_{ou}$ calculated at the unloaded gear.

minor change at the clutch hub component. Especially, the natural frequency relevant to the clutch spring mode related to gear rattle behavior is 102 Hz, which is correlated with the assumed resonance as shown in Fig. 11 well. Thus, the effective clutch stiffness values with the clutch type A are assumed to be increased when the vehicle system is under the coast condition. This indicates that the clutch itself is hitting the stopper regime of the clutch, which will be found out in the nonlinear simulations later.

4.2 Engine torque and drag torque assumptions

Fig. 13 illustrates the input and total drag torques when the vehicle driving condition is changed by the abrupt tip-out of acceleration pedal. Here, t_{o-} and t_{o+} is defined as the moments when the vehicle is driving under the WOT (with tip-in) and coast (with tip-out) conditions respectively. The effective drag torque from all the sub-systems to the flywheel is designated as $T_{DT}(t_{o-})$ (with tip-in) or $T_{DT}(t_{o+})$ (with tip-out) [32]. In order to develop the simulation model, several assumptions are considered as follows: (1) a torsional system is under the steady state condition with the constant input torque when the engine speed is 3000 RPM under the WOT condition; (2) the engine speed is changed abruptly by tipping-out the acceleration pedal. Thus, the vehicle is mostly driven by the inertial torque under the same firing frequency as 100 Hz at 3000 RPM. Only difference is that the torque profiles are changed into the input torque under the idling condition at 700 RPM; (3) the moment when the vehicle system undergoes the abrupt input torque change is defined as $\omega_o t_{o-} \rightarrow \omega_o t_{o+}$. Here, $\omega_o = 2\pi \times 100$ Hz. From the pre-described assumptions and the dynamic

Table 5. List of the input torque profiles under the cost condition at t_{o+} and t_{o-}.

Torque component		Engine speed (RPM)		Effective component of the input torque
		700	3000	
Magnitude (Nm)	T_M	22.0	192.3	-170.3
	T_{p1}	41.5	589.6	548.9
	T_{p2}	14.4	143.3	129.7
	T_{p3}	4.3	53.3	50.7
	T_{p4}	2.7	24.2	24.2
	T_{p5}	1.8	14.1	14.6
	T_{p6}	1.0	8.1	8.6
Phase (rad)	ϕ_{p1}	-1.90	-1.71	1.45
	ϕ_{p2}	-2.69	-2.37	0.81
	ϕ_{p3}	2.25	3.14	0.06
	ϕ_{p4}	0.64	2.18	-0.85
	ϕ_{p5}	-0.38	1.40	-1.62
	ϕ_{p6}	-1.37	0.72	-2.32

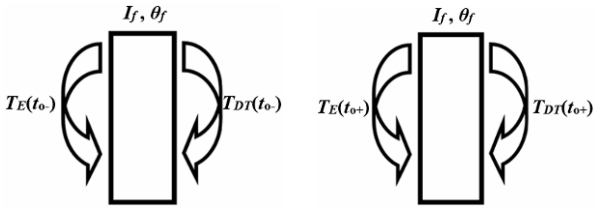

(a) (b)

Fig. 13. Schematics of input and drag torques under tip-in and tip-out conditions: (a) input and total drag torques under the vehicle tip-in condition; (b) input and total drag torques under the vehicle tip-out condition.

behaviors illustrated in Fig. 13, the vehicle system is affected by the effective input torque profiles as follows.

$$T_{Ec}(t_c) = T_E(t_{o+}) + T_{DT}(t_{o+}), \quad (30a)$$

$$T_{DT}(t_{o+}) \approx T_{DT}(t_{o-}) \approx -T_E(t_{o-}), \quad (30b)$$

$$T_E(t_{o-}) = T_{E(3000RPM)}(t), T_E(t_{o+}) = T_{E(700RPM)}(t). \quad (30c,d)$$

Here, the subscript *c*, *700RPM* and *3000RPM* are defined as coast condition, 700 RPM and 3000 RPM of engine speeds respectively. From Eq. 30(b), the total drag torque on the flywheel $T_{DT}(t_{o+})$ is equal to $T_{DT}(t_{o-})$ by assuming that the inertial torque remain with the same magnitudes of $T_{E(3000RPM)}(t)$ right after tipping-out. Thus, the profiles of $T_{DT}(t_{o+})$ is same as $T_E(t_{o-})$ except for the effective direction of the torque. Also, other drag torques in terms of T_{Di}, T_{Do}, T_{Du}, T_{DVE2} shown in Fig. 1 are assumed to still remain with the same values as the properties at t_{o-} due to the inertial torque effect as well. Therefore, only the input torque profiles are changed in terms of the effective input torque profiles described in Table 5 which in-

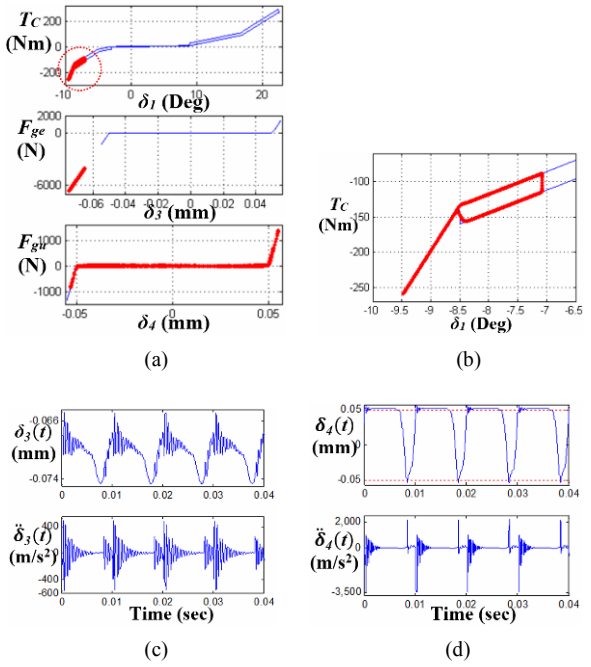

Fig. 14. Clutch torque (or gear mesh forces) and relative displacement with the clutch type A under the coast condition at 3000 RPM: (a) clutch torque (or gear forces) vs. relative displacement; (b) dynamic clutch torque at the stopper regime; (c) relative motions of the engaged gear pair; (d) relative motions of the unloaded gear pair.

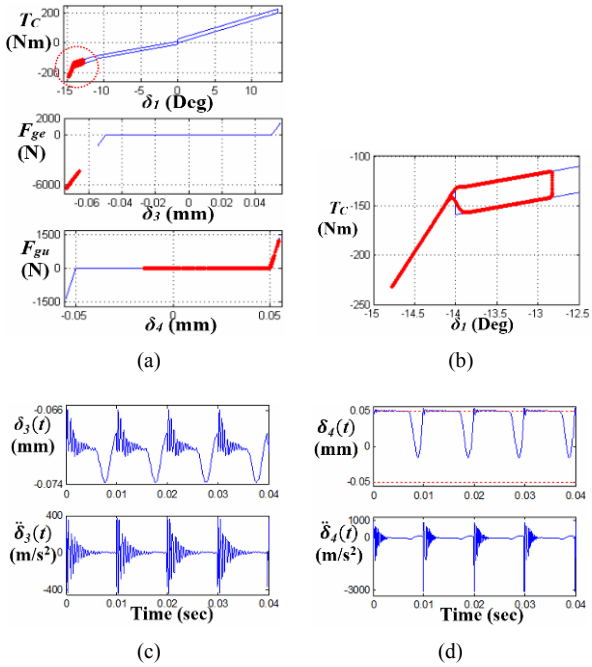

Fig. 15. Clutch torque (or gear mesh forces) and relative displacement with the clutch type B under the coast condition at 3000 RPM: (a) clutch torque (or gear forces) vs. relative displacement; (b) dynamic clutch torque at the stopper regime; (c) relative motions of the engaged gear pair; (d) relative motions of the unloaded gear pair.

cludes the input torque profiles at 700 and 3000 RPM. Thus, the effective component of the engine torque $T_{Ec}(t_c)$ is given by Eqs. 30(a)-(d). Relevant harmonic terms of effective torque profiles $T_{Ec}(t_c)$ are estimated as follows.

$$T_{Ec}(t) = T_{Mc} + \sum_{i=1}^{n} T_{pci} \cos\left(i\Omega_p t + \phi_{pci}\right), \quad (31a)$$

$$T_{Mc} = T_M(t_{o+}) - T_M(t_{o-}), \quad \tilde{T}_{pci} = \tilde{T}_{pi}(t_{o+}) - \tilde{T}_{pi}(t_{o-}), \quad (31b,c)$$

$$\tilde{T}_{pi}(t_{o\pm}) = \cos\left\{\phi_{pi}(t_{o\pm})\right\} + i\tilde{T}_{pi}\sin\left\{\phi_{pi}(t_{o\pm})\right\}. \quad (31d)$$

Here, T_{Mc} and $\tilde{T}_{pci}$ are the effective mean and alternating torques respectively.

4.3 Numerical results under the coast condition

In order to find out the numerical results, Eqs. (25)-(28) can be used by employing $T_{Ec}(t)$ as described in Table 5. When the input conditions are changed between t_{o-} and t_{o+}, several dynamic behaviors are assumed as follows: (1) input torque takes an effect with reverse direction since $T_M(t_{o+})$ is less than $T_M(t_{o-})$ as indicated in Eqs. (30c), (30d) and (32b); (2) thus, all the vehicle dynamics are dependent upon the inertial torque and motions; (3) Initial conditions (ICs) are the same as the values for the WOT condition except for the engaged gear pair since the driving and driven sides of gears are switched due to the torsional direction of input torque. However, all of the drag torques at t_{o+} remain with the same values as at t_{o-}.

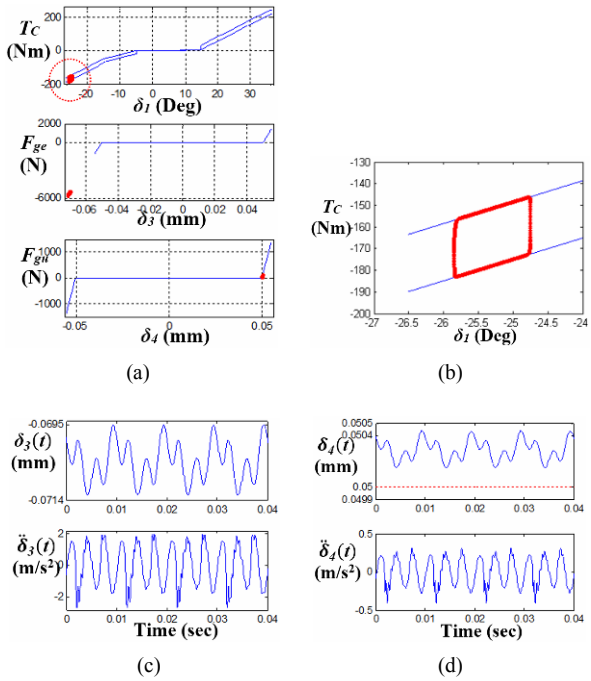

Fig. 16. Clutch torque (or gear mesh forces) and relative displacement with the clutch type C under the coast condition at 3000 RPM: (a) clutch torque (or gear forces) vs. relative displacement; (b) dynamic clutch torque at the stopper regime; (c) relative motions of the engaged gear pair; (d) relative motions of the unloaded gear pair.

Figs. 14-17 show the simulated results of the dynamic characteristics in terms of clutch torque (or gear mesh forces) vs.

Table 6. Simulated peak-to-peak accelerations for each clutch type under the coast condition.

Peak-to-peak acceleration	Clutch type			DMF
	A	B	C	
Engaged gear (m/s^2)	1052.2	808.5	4.67	0.48
Unloaded gear (m/s^2)	5687.1	3961.1	0.73	0.08
Impact type	Double-sided impact	Sing- sided impact	No-impact	No-impact

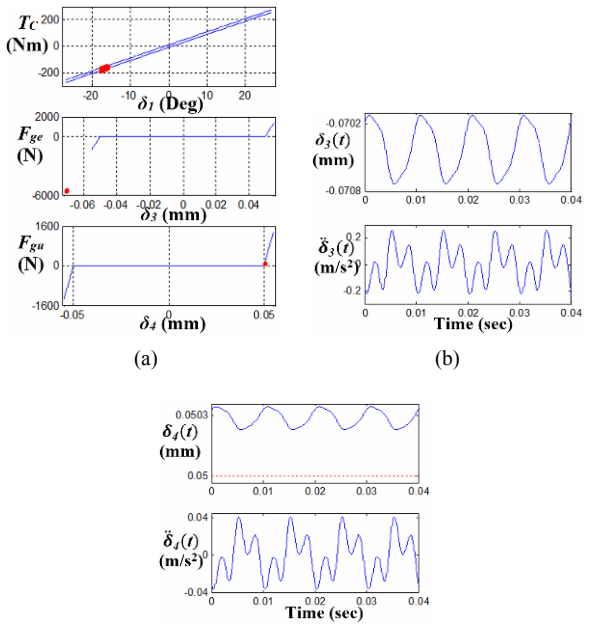

Fig. 17. Clutch torque (or gear mesh forces) and relative displacement with DMF under the coast condition at 3000 RPM: (a) clutch torque (or gear forces) vs. relative displacement; (b) relative motions of the engaged gear pair; (c) relative motions of the unloaded gear pair.

relative displacement and the relative motions in the time domain. The results anticipate the physical motions well. For example, the dynamic clutch torque $T_C\left(\delta_{1\mathrm{pr}}, \dot{\delta}_{1\mathrm{pr}}\right)$ is located on the negative side since the mean effective torque has the minus value from Eq. (31b) and Table 5. The relative motions of the engaged gear pair agree with the dynamic direction well since the engaged gear on the input shaft is physically driven by the inertial torque. However, the unloaded gear pairs still remain under the driving condition as the unloaded gear is always driven by the input shaft. As expected from the measured data and linear analysis previously, Fig. 14 shows clearly that the clutch torque is hitting the stopper at the marginal regime of the transition angle. Also, the unloaded gear pair shows the "double-sided" impact. When the other dynamic characteristics along with the clutch types B and C are compared with DMF case, the wide range of transition angles reduces vibro-impacts. For example, the dynamic behaviors with the clutch types B and C are "single-side" impact and

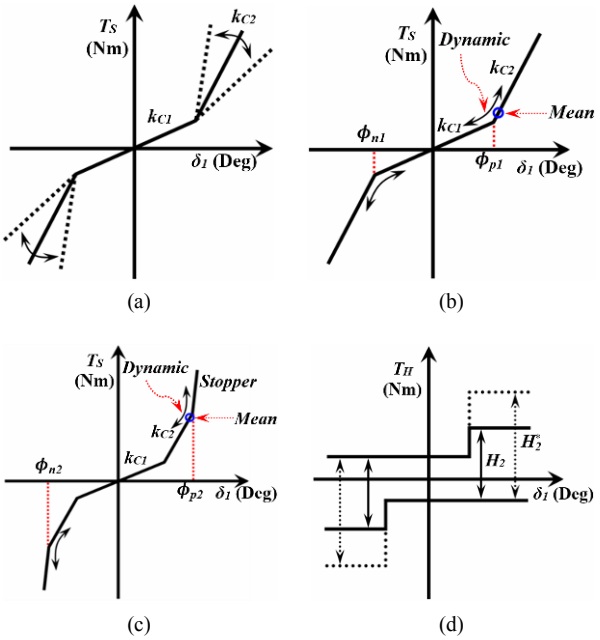

Fig. 18. Key parameters of a clutch damper: (a) a change in stiffness of the second stage; (b) transition angle effect; (c) stopper impact; (d) a change in hysteresis H_2 of the second stage.

"no-impact" respectively. Likewise, the torsional system has no vibro-impact with DMF. As illustrated in Figs. 15(b) and 16(b), the clutch type B has the stopper effect similar to the clutch type A. But the clutch type C has the wide range of transition angles enough to avoid hitting the stopper. In order to simulate the stopper effect, another clutch stiffness value without hysteresis level is employed at the last stage of the transition angle for the clutch types A and B such as −8.51 Deg. and −13.51 Deg. respectively. Here, the employed values are 4 × 3.27 kg·m/deg as used in the linear analysis previously. Table 6 compares the simulated P-P accelerations on the engaged and unloaded gear pairs with the impact type. As shown in Table 6, P-P accelerations of the clutch type A are much higher than the other cases for both engaged and unloaded gear pairs.

DMF can resolve vibro-impacts by employing the more flexible design concepts than the general clutch types. However, when the simulated P-P accelerations of the clutch type C is compared with the DMF case, vibro-impacts also can be resolved by controlling the several design factors. These are explained in the next section.

5. Clutch design guide lines

In the previous sections, several clutch parameters were expected to improve the gear rattle conditions. Based upon the simulations by employing three real-life clutch dampers, several key parameters are considered as shown in Fig. 18. Thus, a clutch damper could be designed to reduce the gear rattle phenomena from some dynamic design principles as follows: (1) use compliant springs as indicated in Fig. 18(a); (2) avoid

Table 7. Characteristics of the modified multi-staged clutch with SMF.

Property		Stage	Values
Torsional stiffness, k_{Ci} (linearized in a piecewise manner (kg·m/deg)		1	0.018
		2	0.11
		3	1.06
Hysteresis, H_i (kg·m)		1	0.1
		2	0.2
		3	2.0
Transition angle, ϕ_i (deg)	Positive side ($\delta > 0$)	1	3.0
		2	9.0
		3	27.0
	Negative side ($\delta < 0$)	1	-3.0
		2	-9.0
		3	-27.0

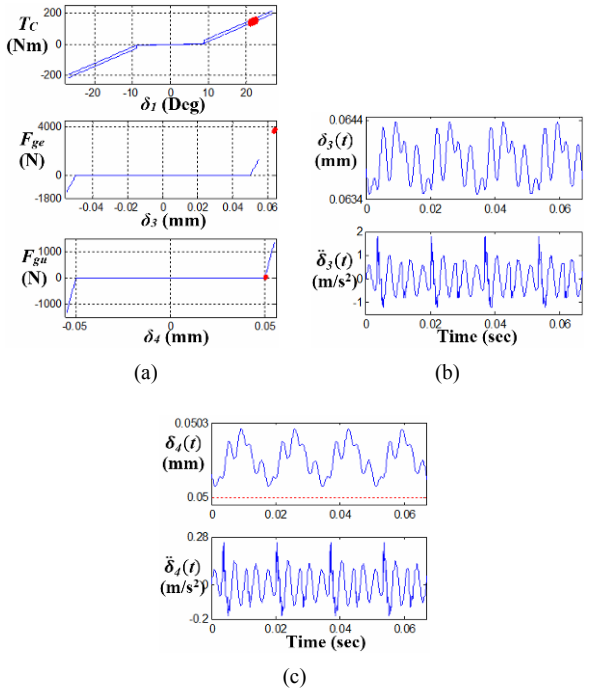

Fig. 19. Clutch torque (or gear mesh forces) and relative displacement with the modified clutch damper under the WOT condition at 1800 RPM: (a) clutch torque (or gear forces) vs. relative displacement; (b) relative motions of the engaged gear pair; (c) relative motions of the unloaded gear pair.

transition regimes illustrated in Fig. 18(b) as the pre-load effect can cause vibro-impacts; (3) do not engage the stopper as illustrated in Fig. 18(c) at the high clutch torque levels; (4) hysteresis values must be relatively high if possible as shown in Fig. 18(d); (5) for the sake of simplicity, the clutch characteristics must be symmetric structure. To implement these suggestions, a modified clutch design is proposed and simulated. Table 7 describes a newly developed clutch damper concept modified from the clutch type A. This illustrates numerical values of the parameters for the modified clutch with a

Table 8. Comparison of simulated accelerations with the modified multi-staged clutch (with SMF) under both WOT and coast conditions.

Simulated Peak-to-Peak acceleration	WOT condition at 1800 RPM	Coast condition at 3000 RPM
Engaged gear (m/s^2)	3.04	3.84
Unloaded gear (m/s^2)	0.43	0.59

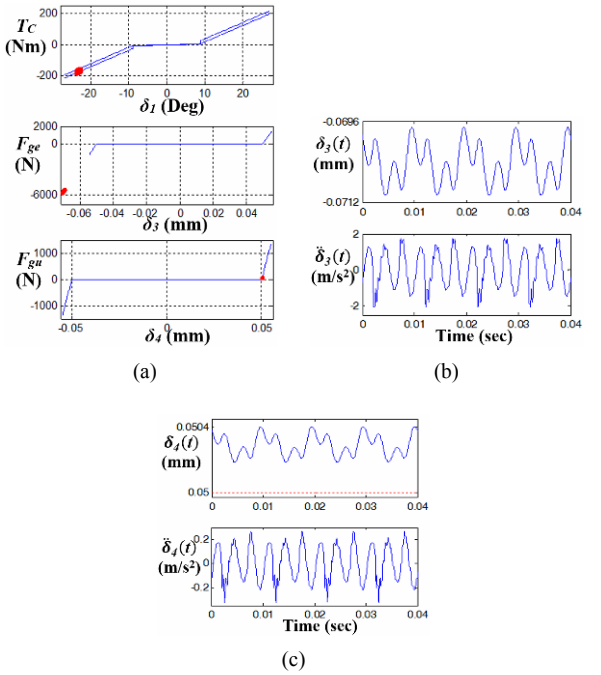

Fig. 20. Clutch torque (or gear mesh forces) and relative displacement with the modified clutch damper under the coast condition at 3000 RPM: (a) clutch torque (or gear forces) vs. relative displacement; (b) relative motions of the engaged gear pair; (c) relative motions of the unloaded gear pair.

symmetric structure and a relatively low-value of k_{C1} and k_{C2}. Also, it has a wide range of transition angles on the last stage which is a dynamic behavior range under the driving condition.

Figs. 19 and 20 show the simulated results in terms of clutch torque (or gear mesh forces) vs. relative displacement and the relative motions in the time domain, with the modified clutch dampers under both WOT (at 1800 RPM) and coast (at 3000 RPM) conditions. In newly designed concepts as shown in Figs. 19(a) and 20(a), small range of transition is designed for a pre-damper regime and a wider displacement range for driving conditions. Therefore, while the system is under both WOT and coast conditions, it operates similar to a linear torsional spring. As observed in Figs. 19 and 20, no rattle is seen on the relationship of clutch torque (or gear mesh forces) vs. relative displacement. Especially, “no-impact” on the unloaded gear pair is clearly observed on the time domain as shown in Figs. 19(c) and 20(c). Table 8 shows simulated results in terms of the P-P accelerations. When these results are compared with the previous simulations shown in Tables 4 and 6, the modified clutch concepts improve the vibro-impacts under

both WOT and coast conditions successfully.

6. Conclusion

This article has investigated the gear rattle phenomena with the 6DOF torsional system model under both WOT and coast conditions. In order to develop a nonlinear simulation model, different clutch dampers and input torque conditions have been considered with focus on the key parameters in the clutch dampers. Specific contributions of this work are summarized as follows. First, the mathematical model for the multi-staged clutch dampers has been developed by including asymmetric transition angles. This advances the nonlinear clutch models suggested by the prior researches [1-7] and it can be employed for any clutch design concepts. Second, the dynamic characteristics along with three real-life clutch designs have been investigated. This leads to the guide lines for the clutch design to improve the torsional vibratory motions into "no-impact" condition. Third, the nonlinear simulation model for the gear rattle under the coast condition has been suggested. Thus, the simulation models for both WOT and coast conditions can be utilized to simulate the gear rattle phenomena along with different vehicle dynamic conditions.

Current work for the improvement of gear rattle condition is focused on the key parameters in a clutch damper. However, this work is limited to suggesting the nonlinear models and simulation method. Therefore, the development of experiment method to reveal the nonlinear dynamic behaviors in a driveline system will be a next stage of work where the comparison of simulation and experiment will be the highlight.

References

[1] T. C. Kim, T. E. Rook and R. Singh, Super- and sub-harmonic response calculation for a torsional system with clearance nonlinearity using the harmonic balance method, *Journal of Sound and Vibration,* 281 (2005) 965-993.

[2] T. C. Kim, T. E. Rook and R. Singh, Effect of nonlinear impact damping on the frequency response of a torsional system with clearance, *Journal of Sound and Vibration,* 281 (2005) 995-1021.

[3] T. C. Kim, T. E. Rook and R. Singh, Effect of smoothening functions on the frequency response of an oscillator with clearance non-linearity, *Journal of Sound and Vibration,* 263 (2003) 665-678.

[4] T. E. Rook and R. Singh, Dynamic analysis of a reverse-idler gear pair with concurrent clearance, *Journal of Sound and Vibration,* 182 (2) (1995) 303-322.

[5] C. Padmanabhan and R. Singh, Analysis of periodically excited non-linear systems by a parametric continuation technique, *Journal of Sound and Vibration,* 184 (1) (1995) 35-58.

[6] E. P. Trochon, Analytical formulation of automotive drive-train rattle problems, *MS Thesis*, The Ohio State University (1997).

[7] R. Singh, H. Xie and R. J. Comparin, Analysis of automotive neutral gear rattle, *Journal of Sound and Vibration,* 131 (2) (1989) 177-196.

[8] M. Barthod, B. Hayne, J. L. Tebec and J. C. Pin, Experimental study of gear rattle excited by a multi-harmonic excitation, *Applied Acoustics,* 68 (2007) 1003-1025.

[9] M. Y. Wang, W. Zhao and R. Manoj, Numerical modeling and analysis of automotive transmission rattle, *Journal of Vibration and Control,* 8 (2002) 921-943.

[10] S. B. Shim, Y. J. Park and K. U. Kim, Reduction of PTO rattle noise of an agricultural tractor using an anti-backlash gear, *Biosystems Engineering,* 100 (2008) 346-354.

[11] E. Rocca and R. Russo, Theoretical and experimental investigation into the influence of the periodic backlash fluctuations on the gear rattle, *Journal of Sound and Vibration,* 330 (2011) 4738-4752.

[12] K. Karagiannis and F. Pfeiffer, Theoretical and experimental investigations of gear-rattling, *Nonlinear Dynamics,* 2 (1991) 367-387.

[13] M. Bozca and P. Fietkau, Empirical model based optimization of gear box geometric design parameters to reduce rattle noise in an automotive transmission, *Mechanism and Machine Theory,* 45 (2010) 1599-1612.

[14] O. Tangasawi, S. Theodossiades and H. Rahnejat, Lightly loaded lubricated impacts: Idle gear rattle, *Journal of Sound and Vibration,* 308 (2007) 418-430.

[15] C. Padmanabhan and R. Singh, Spectral coupling issues in a two-degree-of-freedom system with clearance non-linearities, *Journal of Sound and Vibration,* 155 (2) (1992) 209-230.

[16] C. Padmanabhan, R. C. Barlow, T. E. Rook and R. Singh, Computational issues associated with gear rattle analysis, *Tran. ASME Journal of Mechanical Design,* 117 (1995) 185-192.

[17] R. J. Comparin and R. Singh, Non-linear frequency response characteristics of an impact pair, *Journal of Sound and Vibration,* 134 (2) (1989) 259-290.

[18] R. J. Comparin and R. Singh, Frequency response characteristics of a multi-degree-of-freedom system with clearance, *Journal of Sound and Vibration,* 142 (1) (1990) 101-124.

[19] C. Padmanabhan and R. Singh, Dynamics of a piecewise non-linear system subject to dual harmonic excitation using parametric continuation, *Journal of Sound and Vibration,* 184 (5) (1995) 767-799.

[20] T. C. Kim and R. Singh, Dynamic interactions between loaded and unloaded gears, *Tans. SAE,* 110 (6) (2001) 1934-1943.

[21] P. Couderc, J. Callenaere, J. D. Hagopian and G. Ferraris, Vehicle driveline dynamic behavior: experimentation and simulation, *Journal of Sound and Vibration,* 218 (1) (1998) 133-157.

[22] Y. Chikatani and A. Suehiro, Reduction of idling rattle noise in trucks, *SAE 911044* (1991) 49-56.

[23] T. P. Howell, N. N. Powell and P. Etheridge, The application of correlated modeling techniques to investigate gear rattle noise in a Harley-Davidson motorcycle, *Inter-Noise*

2002 proceedings (2002) 19-21.
[24] T. Shimizu, Mechanism of the idle gear rattle synchronized with engine rotation, *SAE 932003* (1993) 7-13.
[25] A. Laschet, Computer simulation of vibration in vehicle powertrains considering nonlinear effects in clutches and manual transmissions, *SAE 941011* (1994) 1-8.
[26] J. Fan, P. Hierlwimmer and A. Laschet, Investigation of gear rattle sensitivity on manual transmissions in the target setting process, *ATZ Automobiltechnische Zeitschrift* (1997) 9-11.
[27] C. Padmanabhan, T. E. Rook and R. Singh, Modeling of automotive gear rattle phenomenon: State of the art, *SAE 951316* (1995) 669-680.
[28] C. Padmanabhan and R. Singh, Influence of clutch design on the reduction and perception of automotive transmission rattle noise, *Noise-Con 93 proceedings* (1993) 607-612.
[29] J. P. D. Hartog, *Mechanical vibrations*, Dover, PA, USA (1985).
[30] J. Y. Yoon and R. Singh, Dynamic force transmitted by hydraulic mount: Estimation in frequency domain using motion and/or pressure measurements and quasi-linear models, *Noise Control Engineering Journal,* 58 (4) (2010) 403-419.
[31] J. R. Dormand and P. J. Prince, A family of embedded Runge-Kutta formulae, *Journal of Computational and Applied Mathematics,* 6 (1) (1980) 19-26.
[32] C. L. Gaillard and R. Singh, Dynamic analysis of automotive clutch dampers, *Applied Acoustics,* 60 (4) (2000) 399-424.

Jong-Yun Yoon received his Ph.D. from the Department of Mechanical Engineering at the Ohio State University. He is currently an assistant professor at Kongju National University. His research interests are in automotive NVH, including nonlinear torsional vibration.

Byeongil Kim received his Ph.D. from the Department of Mechanical Engineering at the Ohio State University. He is currently an assistant professor at Yeungnam University. His research interests are smart structures and vibration control, especially in automotive NVH applications.